NeuroImage 71 (2013) 298–306

Contents lists available at SciVerse ScienceDirect

NeuroImage

journal homepage: www.elsevier.com/locate/ynimg

Classifying fMRI-derived resting-state connectivity patterns according to their daily rhythmicity

Janusch Blautzik [a], Céline Vetter [b], Isabella Peres [a,b], Evgeny Gutyrchik [b,c], Daniel Keeser [a,d], Albert Berman [a], Valerie Kirsch [a,e], Sophia Mueller [a], Ernst Pöppel [b,c], Maximilian Reiser [a], Till Roenneberg [b,*], Thomas Meindl [a]

[a] Institute of Clinical Radiology, Ludwig-Maximilians-University, Munich, Germany
[b] Institute of Medical Psychology, Ludwig-Maximilians-University, Munich, Germany
[c] Human Science Centre, Ludwig-Maximilians-University, Munich, Germany
[d] Department of Psychiatry, Ludwig-Maximilians-University, Munich, Germany
[e] Department of Neurology, Ludwig-Maximilians-University, Munich, Germany

ARTICLE INFO

Article history:
Accepted 6 August 2012
Available online 14 August 2012

Keywords:
Circadian rhythm
Homeostatic process
Resting-state networks
Functional magnetic resonance imaging
MCTQ

ABSTRACT

The vast majority of biological functions express rhythmic fluctuations across the 24-hour day. We investigated the degree of daily modulation across fMRI (functional Magnetic Resonance Imaging) derived resting-state data in 15 subjects by evaluating the time courses of 20 connectivity patterns over 8 h (4 sessions).
For each subject, we determined the chronotype, which describes the relationship between the individual circadian rhythm and the local time. We could therefore analyze the daily time course of the connectivity patterns controlling for internal time. Furthermore, as the participants' scan times were staggered as a function of their chronotype, we prevented sleep deprivation and kept time awake constant across subjects. Individual functional connectivity within each connectivity pattern was defined at each session as connectivity strength measured by a mean z-value and, in addition, as the spatial extent expressed by the number of activated voxels.
Highly rhythmic connectivity patterns included two sub-systems of the Default-Mode Network (DMN) and a network extending over sensori-motor regions. The network characterized as the most stable across the day is mainly associated with processing of executive control.
We conclude that the degree of daily modulation largely varies across fMRI derived resting-state connectivity patterns, ranging from highly rhythmic to stable. This finding should be considered when interpreting results from fMRI studies.

© 2013 Elsevier Inc. All rights reserved.

Introduction

The vast majority of biological functions express rhythmic fluctuations across the 24-hour day. Examples for this include gene expression (Merrow et al., 2005), plasma concentration of hormones (Czeisler and Klerman, 1999), core body temperature (Cagnacci et al., 1992; Refinetti and Menaker, 1992), and higher cognitive functions (Schmidt et al., 2007). The waveform of these daily rhythms can in most cases be described by a two-harmonic regression model combining a 24- and a 12-hour component (Brown and Czeisler, 1992).

Daily rhythms in sleep and activity, and consequently also in the modulation of other daily rhythms, are caused by an interaction between circadian rhythmicity and time awake (homeostatic process). Circadian rhythms are self-sustained oscillatory processes, which are actively synchronized (entrained) to the 24-hour day — predominantly by the light/dark cycle (Roenneberg and Merrow, 2005). The relationship between the external temporal environment and the individual circadian rhythm (phase of entrainment) is highly individual, giving rise to so-called 'chronotypes' (Roenneberg et al., 2003, 2012). The homeostatic process describes the accumulation of sleep pressure during the wake period, decreasing during sleep (Borbely, 1982; Rogers et al., 2003; Schmidt et al., 2007).

Systematic investigations of daily rhythmicity in neural activity are rare, but the available data suggests that brain activity also fluctuates over the course of a day — at least in specific brain areas. This has been shown, for example, as differences in regional brain glucose metabolism between morning and evening scans using [^{18}F]-fluorodeoxyglucose positron emission tomography (Buysse et al., 2004) or as significant daily changes in cortical activity using low-resolution brain electromagnetic tomography (Toth et al., 2007). Moreover, Schmidt et al. (2009) have demonstrated in a functional Magnetic Resonance Imaging (fMRI) experiment that activity in the suprachiasmatic nucleus in the hypothalamus is associated with both chronotype and the homeostatic process. Recently, we reported the influence of chronotype on the daily activity

* Corresponding author at: Institute of Medical Psychology, Ludwig-Maximilians-University Munich, Goethestr. 31, 80336 Munich, Germany. Fax: +49 89 2180 75616.
E-mail address: till.roenneberg@med.uni-muenchen.de (T. Roenneberg).

1053-8119/$ – see front matter © 2013 Elsevier Inc. All rights reserved.
http://dx.doi.org/10.1016/j.neuroimage.2012.08.010

of specific brain areas during a simple fMRI motor task (Peres et al., 2011).

So far, rhythmic daily fluctuations have not been reported for resting-state networks (RSNs), which represent brain regions of synchronized low-frequency (0.01–0.1 Hz) fluctuations in the blood oxygen level dependent (BOLD) signal measured by fMRI during resting-state conditions (Beckmann et al., 2005; Biswal et al., 2010; Damoiseaux et al., 2006). Although little is known about the physiological significance of RSNs, the available data suggests that these intrinsic connectivity patterns reflect ongoing neural activity, which may play a role in maintaining the brain's functional integrity (Brookes et al., 2011; He et al., 2008; Miall and Robertson, 2006; Pizoli et al., 2011; Shmuel and Leopold, 2008).

Apart from the RSN's potential importance for core brain functions, numerous reports show that connectivity changes within these systems are associated with pathological conditions such as neuropsychiatric and neurodegenerative disorders, e.g. Alzheimer's disease (Greicius et al., 2004; Rombouts et al., 2005; Sorg et al., 2007; Zhang et al., 2010), autism (Stigler et al., 2011), or multiple sclerosis (Rocca et al., 2010). These findings may suggest the application of resting-state fMRI for clinical purposes.

So far, both scientific and clinical applications rely on the hypothesis that RSNs remain stable across the day. Knowledge about potential daily fluctuations would however be fundamental for the interpretation of fMRI results. We therefore explored the daily time course of fMRI derived resting-state connectivity patterns, while controlling for inter-individual variation in internal time (i.e., chronotype) and time-awake (i.e., the homeostatic process).

Experimental procedures

Participants

Fifteen young, healthy volunteers participated in the study (9 female subjects; age: 23.0 ± 3.0 years). Right-handedness was ensured by a minimum Lateralization Quotient of 70, as assessed with the Edinburgh Inventory (Oldfield, 1971). Psychiatric or neurological disease and sleep disorders were exclusion criteria as well as intra-corporal ferromagnetic objects, shift work or psychoactive substance abuse within the last three months, current or previous drug addiction, and smoking. Female participants took a urine ß-HCG test to exclude pregnancy.

The study was carried out in accordance with the Declaration of Helsinki. It was reviewed and approved by the university's local ethics committee. All subjects gave their informed consent and received payment for their participation.

Assessment of internal time

The Munich ChronoType Questionnaire (MCTQ) enables the reliable quantification of chronotype by determining an individual's "mid-sleep time on free days" (MSF), corrected for potential sleep debt accumulated during the work week (MSF_{sc}; Roenneberg et al., 2003, 2007, 2012; Wittmann et al., 2006). "Mid-sleep on free days" refers to the midpoint between sleep onset and sleep offset on free days; if participants sleep less on work days than on free days, MSF is corrected for "over-sleep", resulting in MSF_{sc}:

$$MSF = \text{Sleep Onset} + (\text{Sleep duration on free days})/2$$

$$MSF_{sc} = MSF - (\text{Sleep duration on free days} - \text{average weekly sleep duration})/2.$$

Only intermediate to moderately late chronotypes (MSF_{sc}: 3–7) were included in the study. Subjects kept sleep-logs for 10 days prior to the experiment to validate the chronotype (Roenneberg et al., 2007; Wittmann et al., 2006) and to determine an individual's time awake for each session. Additionally, participants wore wrist actimeters (Daqtometer Version 2.3, Daqtix GbR, Oetzen, Germany) during the same period to objectively record activity–rest cycles; actimetry data were consolidated in 10-min bins and a weighted "center of gravity" (Cog; Kenagy, 1980) was averaged across the 10-day period as a physiological phase-indicator.

For validation purposes, we correlated the MCTQ derived chronotype (MSF_{sc}) with the sleep-log based average mid-sleep (weighted as a function of work and free days) as well as with the averaged CoGs. Data evaluation and validation were performed with SPSS Statistics 19.0, Microsoft Excel, and ChronOSX 2.0 (Roenneberg and Taylor, 2000).

Study design

Functional MRI scans were performed at fixed intervals of 2.5 h, starting at 9.00 a.m. Individual scanning times were adapted to the participant's MSF_{sc} to minimize chronotype differences and to keep time awake as similar as possible. Early chronotypes (MSF_{sc}: 3.0–4.0) were measured first, followed by those with an MSF_{sc} between 4.0 and 5.0, then those with an MSF_{sc} between 5.0 and 6.0, and finally those with an MSF_{sc} between 6.0 and 7.0. Since the study design did not allow to measure similar chronotypes at the same local time on the same day, measurements were spread out over several days. During scanning, subjects were instructed to keep their eyes closed without falling asleep and not to think of anything in particular. We chose this study design to control for the individuals' time-awake. Given the regular 2.5 h intervals between scans, this procedure should lead to a good relationship between internal time (i.e., h since MSF_{sc}) and time-awake at the respective measurement times. This was evaluated post-hoc by a Pearson's correlation analysis.

Measurements were taken on four weekends during the summer; to ensure equal inter-day testing conditions, subjects were instructed to stay in the windowless waiting area for the duration of the entire experiment since daylight exposure is known to affect the circadian phase and neural activation (Roenneberg and Foster, 1997; Roenneberg et al., 2007; Vandewalle et al., 2006, 2007a). Light snacks and beverages were provided ad libitum. Caffeine intake was not controlled for, subjects were however told to consume caffeinated beverages during the study day as they normally do.

Functional magnetic resonance imaging

Functional MRI was performed using a 3.0 Tesla Magnetom (VERIO, Siemens, Erlangen, Germany) with a 12-element head coil. For anatomical reference, a sagittal high-resolution magnetization-prepared rapid gradient-echo sequence (MPRAGE) was acquired with the following imaging parameters: field of view (FoV): 256 × 256 mm; spatial resolution: 1 × 1 × 1 mm; time of repetition (TR): 2400 ms; time of echo (TE): 3,06 ms; flip angle (FA): 9°; number of slices: 160; and acquisition time (TA): 4:45 min. Functional data were recorded by means of a BOLD sensitive echo-planar gradient-echo sequence in axial orientation (FoV: 192 × 192 mm; spatial resolution: 3 × 3 × 4 mm; slice gap: 0.4 mm; imaging matrix: 64 × 64; TR: 3000 ms; TE: 30 ms; FA: 80°; number of slices: 36; TA: 6:06 min). Before starting imaging, 3D-field shimming was performed using automated shimming algorithms implemented on the scanner.

Statistical analyses of functional MRI data

Data processing and statistical analyses were carried out using FSL (FMRIB Software Library, http://www.fmrib.ox.ac.uk/fsl/index.html) version 4.1.7 and AFNI (Analyses of Functional Images, http://afni.nimh.nih.gov/afni).

Data preprocessing

The initial five volumes of every functional run were discarded to account for T1 saturation effects. Pre-statistics processing was done in four steps: (1) individual high-resolution T1-weighted images were processed using AFNI; (2) head motion correction was performed using MCFLIRT (Motion Correction using FMRIB's Linear Image Registration Tool) (Jenkinson et al., 2002); (3) the skull was removed using BET (Brain Extraction Tool) (Smith, 2002) followed by spatial smoothing using a 5-mm FWHM Gaussian kernel with high-pass temporal filtering (Gaussian-weighted least squares straight line fitting with sigma = 100 s); and (4) registration of functional data to the corresponding individual high-resolution T1-weighted images and transformation to the MNI152 standard brain space were performed applying FLIRT (FMRIB's Linear Image Registration) version 5.5 (Jenkinson et al., 2002).

Independent component analysis

Functional MRI data was analyzed using MELODIC (Multivariate Exploratory Linear Optimized Decomposition into Independent Components) software, version 3.10 in combination with a dual-regression analysis as implemented in FSL 4.1.7 (Beckmann et al., 2009; Biswal et al., 2010). This approach has been recently demonstrated to generate highly reliable and reproducible independent components (ICs) over the short- and long-term run (Zuo et al., 2010).

Functional MRI derived time-courses of all participants (15) and sessions (4) – a total of 60 scans – were spatially concatenated in the MNI152 standard space for allowing the estimation of a covariance matrix, which was used for reduction of individual data sets via Probabilistic Independent Component Analysis. Reduced individual data sets were further processed with Temporal Concatenation Group ICA (TC-GICA) to calculate group-level component maps across all subjects and sessions. In agreement with prior studies, we used a lower order TC-GICA fixing the number of components to 20 (Biswal et al., 2010; Smith et al., 2009; Zuo et al., 2010).

Only previously described RSNs in functionally relevant brain areas (Biswal et al., 2010; Damoiseaux et al., 2006; Laird et al., 2011; Zuo et al., 2010) with low frequency signals in the range of 0.01–0.1 Hz (Boly et al., 2008; Fox et al., 2005; Greicius et al., 2003; Horovitz et al., 2009; Vincent et al., 2007) were considered as RSNs in this study; connectivity patterns not meeting these criteria were considered as non-neural noise (Dagli et al., 1999; Lund et al., 2006).

The TC-GICA derived multi-subject multi-session ICs were reconstructed into individual ICs for each subject and session (resulting in a total of 1200 individual ICs) applying the dual regression approach (Biswal et al., 2010; Filippini et al., 2009; Zuo et al., 2010).

Rhythmicity assessment in resting-state connectivity patterns

We investigated the relative rhythmicity of each connectivity pattern as a function of internal time, i.e., based on hours elapsed since MSF_{sc}. For this purpose, mean z-values representing the connectivity strength within a statistical component map were extracted from each individual IC. In order to exclude statistically non-relevant activations from this analysis, i.e., voxels not representing a connectivity pattern with a high degree of probability, we defined a threshold of $z \geq 3.0$ for the individual ICs, which equals a conservative significance level of $p \leq 0.0027$. In addition, we calculated the spatial extent of each connectivity pattern by extracting the number of activated voxels within each individual IC thresholded at $z \geq 3.0$. For validation purposes, mean z-values were complementarily extracted from connectivity patterns that were generated at different threshold levels ($z \geq 1.0$ and $z \geq 2.0$) and from a threshold-free mask-based approach. For the latter approach, we imposed the connectivity patterns represented in Fig. 2 as masks on corresponding (unthresholded) individual ICs; the average z-score per individual connectivity pattern was then extracted from the brain regions located within that mask.

To control for inter-individual differences in baseline connectivity levels, z-values and the number of voxels were then expressed as % deviation from individual mean across all four scan sessions (see Appendix A for variation of the data). We then modeled the daily time course of functional connectivity within each (group-level) connectivity pattern by applying the two-harmonic equation

$$f(\psi) = a \cdot \cos(\psi) + b \cdot \sin(\psi) + c \cdot \cos(2\psi) + d \cdot \sin(2\psi) + e$$

(Box and Jenkins, 1970; Brown and Czeisler, 1992) to the individual % deviations plotted against h since MSF_{sc}.

We thereby obtained a regression coefficient (r) of the fitting function for each connectivity pattern, as well as its range of oscillation (maximum of the best fit–minimum of the best fit). Rhythmicity of a given signal is characterized by both its range of oscillation and the goodness of fit (i.e., r), which highly correlate (Fig. 1). To quantify the inherent strength of rhythmicity, we used a 'Rhythmicity Index' (RI, by multiplying 'r' with the range of oscillation; RIs were multiplied by 100 for visualization purposes).

Connectivity patterns were ranked according to their RIs, from most rhythmic to most stable. A connectivity pattern was characterized as highly rhythmic when its RI was above 1.5 standard deviations from the average RI across all connectivity patterns. Those with RIs below that cut-off were considered as stable.

Results

All subjects showed good tolerance of the fMRI experiments, so that we were able to collect complete time series from all. Data sets were not constrained by motion artifacts; therefore, all data were used for further analysis.

Internal time

The MCTQ derived chronotype (mean MSF_{sc}: 5.2 ± 1.1) correlated highly with the weighted mid-sleep times calculated from the sleep-log ($r = 0.80$; $p < 0.001$), suggesting that participants were

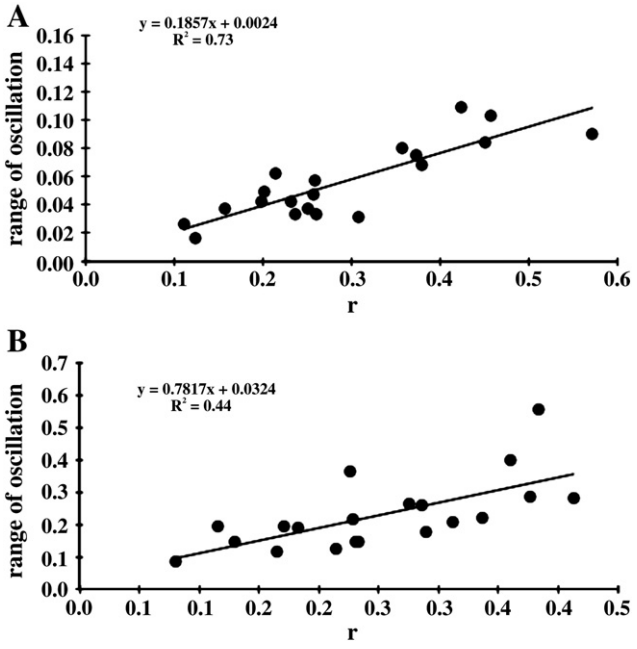

Fig. 1. Correlation between the range of oscillation and r. Association between r (abscissa) and the range of oscillation (ordinate) of the respective fitting functions of the 20 ICs on the basis of all 15 subjects for (A) connectivity strength (mean z-value) with $R^2 = 0.73$ ($p < .001$) and (B) spatial extent (number of voxels) with $R^2 = 0.44$ ($p < .001$). Data are based on individual connectivity patterns thresholded at $z \geq 3.0$.

adequately categorized within the staggered study design. A significant correlation was observed between the weighted mid-sleep and the average center of gravity as determined by actimetry data ($r = 0.66$, $p < 0.01$). As expected, there was also a high correlation between internal time (h elapsed since MSF_{sc}) and time awake across the four sessions ($r = 0.97$).

Functional MRI data

Across the twenty multi-subject, multi-session ICs (Fig. 2) obtained by the TC-GICA approach, we considered 16 connectivity patterns as RSNs; 4 patterns were considered to represent non-neural physiological noise, such as pulsation of cerebrospinal fluid (IC 1) (Lund et al., 2006; Zuo et al., 2010) or large vessels including draining veins (IC 2 & 18) (Dagli et al., 1999; Zuo et al., 2010), and head motion due to cardiac or respiratory pulsation (IC 9) (Dagli et al., 1999; Lund et al., 2006; Zuo et al., 2010). All designated RSNs were highly consistent with previously reported connectivity patterns (Biswal et al., 2010; Damoiseaux et al., 2006; Laird et al., 2011; Zuo et al., 2010) and extended symmetrically over both hemispheres, except for patterns represented in IC 8 and 19.

IC 3 showed a widespread connectivity pattern including the anterior and posterior cingulate gyrus, the precuneus cortex, the supra-marginal gyrus, the lateral occipital cortex, and the insular/operculum cortex. Both IC 4 and 11 involved pre- and post-central gyri (Biswal et al., 1995, 2010). Connectivity patterns represented in IC 5, 14 and IC 17 were similar to the classic default-mode network (DMN) described by Raichle et al. (2001); the three ICs showed a connectivity pattern extending over the precuneus cortex, the posterior and anterior cingulate gyrus, the ventromedial prefrontal cortex, and parietal regions. Connectivity represented in IC 5 and 17 was pronounced in dorsal regions (see Appendix B), whereas IC 14 showed a predominantly frontal connectivity pattern. The division of the DMN into subsystems is in line with prior studies (Biswal et al., 2010; Zuo et al., 2010). IC 6 predominantly comprised the anterior cingulate gyrus extending into the superior frontal gyrus, the frontal pole, and the insular/frontal operculum cortex; IC 7 combined the superior parietal cortex extending into the occipital pole with pre-central regions; this connectivity pattern has been described as the dorsal attention network (Fox et al., 2006). ICs 8 and 19 were characterized by a primarily lateralized fronto-temporo-parietal connectivity pattern in both hemispheres (Biswal et al., 2010). ICs 10, 12 and 15 included areas within the medial and/or visual cortex (Smith et al., 2009). A connectivity pattern predominantly extending over the cerebellum, the thalami and the basal ganglia was represented in IC 13; in the current study this connectivity pattern was not divided into two components as reported by others (Biswal et al., 2010; Laird et al., 2011). IC 16 showed a connectivity pattern mainly involving the middle temporal gyrus extending into the angular gyrus with additional involvement of the precuneus cortex and prefrontal regions; this connectivity pattern has been described as another sub-system of the DMN (Zuo et al., 2010). IC 20 encompassed regions predominantly located in the orbitofrontal cortex; although this connectivity pattern resembles to previously described RSNs (Biswal et al., 2010; Zuo et al., 2010), it may also represent a movement-by-field-inhomogeneity artifact (Andersson et al., 2001; Drobnjak et al., 2006).

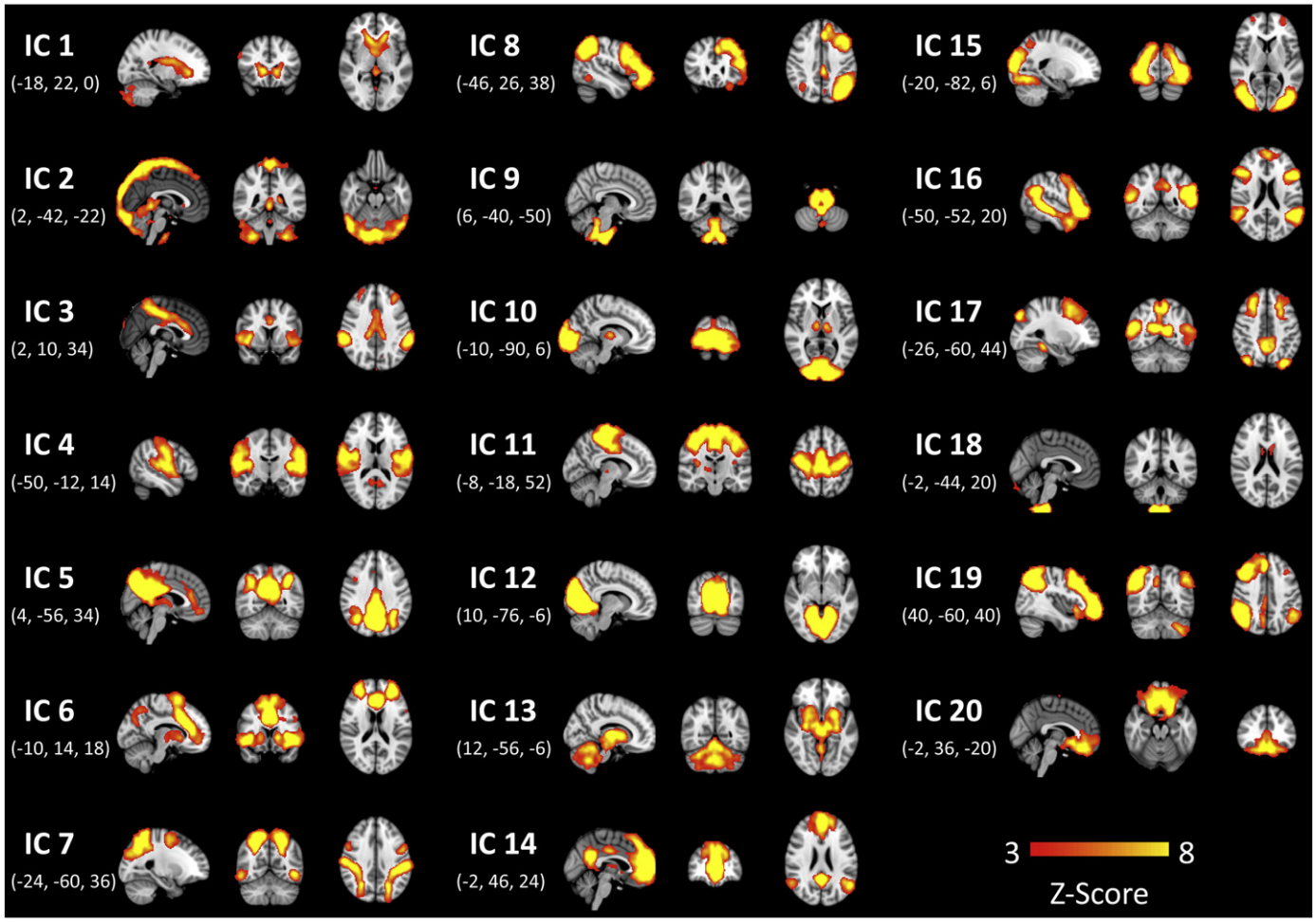

Fig. 2. Multi-subject multi-session independent components. Component maps for all 15 subjects and 4 sessions as generated by the TC-GICA sorted by the decreasing percentage of variance explained by each component. Representative sagittal, coronal and axial images of each multi-subject multi-session statistical map are displayed in radiological convention (x-, y-, and z-coordinates of each slice in the MNI152 standard space are given in parenthesis).

Some of the areas represented in these RSNs may overlap with 'activations' suggested to derive from variations in the depth and rate of respiration (Birn et al., 2006; Chang and Glover, 2009; Wise et al., 2004); we will refer to this topic in the discussion.

Classifying connectivity patterns

Table 1 shows the classification of the 20 connectivity patterns as a function of RI. The cut-off (mean RI + 1.5 SD) was 4.08 for the connectivity strength (mean RI = 1.86 ± 2.2), and 13.47 for the spatial extent (mean RI = 6.21 ± 7.26). Since RI − 1.5 SD produced negative values, we only classified the least rhythmic connectivity patterns as most stable (Fig. 3).

Regarding connectivity strength, we identified at the threshold of $z \geq 3.0$ three highly rhythmic connectivity patterns (all of them considered as RSNs): ICs 5, 11, and 17. Note that in addition to fulfilling the criterion (RI > mean RI + 1.5 SD), the two-harmonic fits were significant in all three RSNs. Although the RI of IC 13 fell below the cut-off, this pattern also showed a significant fit (Fig. 4 and Table 1).

Two of the top rhythmic RSNs identified in the context of connectivity strength (ICs 5 & 17) were also classified as highly rhythmic in the context of their spatial extent, although the two-harmonic regression model produced no significant fits after Bonferroni correction for multiple regressions (Table 1, right panel and Fig. 5); the RIs of ICs 11 & 13 (the next highest in the ranking) fell below the cut-off.

IC 6 and IC 18 showed the least rhythmic daily kinetics for both connectivity strength and spatial extent (though with inverse ranks), indicating them as the two most stable among the 20 identified connectivity patterns (Fig. 6).

ICs 5 and 17 oscillated in phase (for both connectivity strength and spatial extent), with a peak at the first scanning time (i.e., 4 to 6 h after MSF_{sc}) followed by a decline throughout the day and a rising again towards the evening.

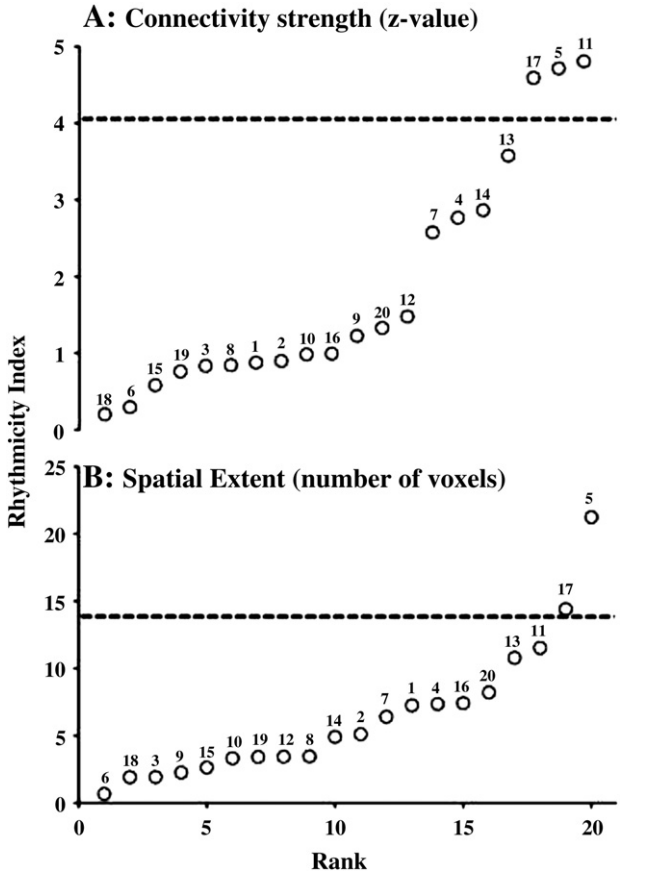

Fig. 3. Relationship between ranks and Rhythmicity Index. The figure depicts the relationship between the ranking of a connectivity pattern (abscissa) and the Rhythmicity Index (ordinate) for both the connectivity strength (A) and the spatial extent (B). The most rhythmic connectivity patterns according to the Rhythmicity Index are localized above the upper dashed line, which represents the chosen threshold of average Rhythmicity Index + 1.5 standard deviations.

Table 1
Fit parameters, rhythmicity index (RI) and ranking of the connectivity patterns.

Connectivity strength						Spatial extent					
IC	r-Value	p-Value	Amp	RI	Rank	IC	r-Value	p-Value	Amp	RI	Rank
1	0.25	0.0536	0.03	0.88	14	1	0.27	0.0339	0.26	7.02	8
2	0.31	0.0171	0.03	0.90	13	2	0.29	0.0250	0.16	4.75	11
3	0.26	0.0459	0.03	0.83	16	3	0.17	0.2039	0.12	1.91	18
4	0.37	0.0035	0.07	2.77	6	4	0.34	0.0087	0.21	7.08	7
5	0.46	0.0002*	0.10	4.71	2	5	0.38	0.0025	0.55	21.22	1
6	*0.11*	*0.3958*	*0.03*	*0.30*	*19*	*6*	*0.08*	*0.5373*	*0.08*	*0.68*	*20*
7	0.38	0.0029	0.07	2.57	7	7	0.31	0.0155	0.20	6.10	9
8	0.20	0.1289	0.04	0.84	15	8	0.18	0.1599	0.19	3.45	12
9	0.26	0.0483	0.05	1.22	10	9	0.12	0.3733	0.19	2.25	17
10	0.20	0.1234	0.05	0.98	12	10	0.17	0.1913	0.19	3.32	13
11	0.57	0.0000*	0.08	4.81	1	11	0.41	0.0010	0.26	10.61	3
12	0.26	0.0469	0.06	1.48	8	12	0.23	0.0729	0.14	3.21	15
13	0.45	0.0003*	0.08	3.57	4	13	0.38	0.0031	0.27	10.06	4
14	0.36	0.0052	0.08	2.86	5	14	0.23	0.0792	0.21	4.87	10
15	0.16	0.2289	0.04	0.58	18	15	0.21	0.0998	0.12	2.51	16
16	0.23	0.0745	0.04	0.99	11	16	0.29	0.0272	0.26	7.41	6
17	0.42	0.0008*	0.11	4.59	3	17	0.36	0.0048	0.40	14.42	2
18	*0.12*	*0.3460*	*0.02*	*0.20*	*20*	*18*	*0.13*	*0.3201*	*0.14*	*1.87*	*19*
19	0.24	0.0702	0.03	0.76	17	19	0.23	0.0755	0.14	3.26	14
20	0.21	0.1010	0.06	1.33	9	20	0.23	0.0831	0.36	8.21	5

Parameters and rankings are given for all connectivity patterns, with regard to both, connectivity strength (left panel) and spatial extent (right panel). Data are derived from individual ICs thresholded at $z \geq 3.0$. Connectivity patterns with a significant rhythmicity, as defined by an outlier approach (see Experimental procedures), are highlighted in gray; the least rhythmic connectivity patterns are italicized. r-Value: coefficient of the fitting function; p-value: significance of the fitting function; Amp: amplitude or range of oscillation of the fitting function (max–min); RI: rhythmicity index (r-value∗Amp∗100); and rank: rank as a function of RI among the 20 connectivity patterns with 1 indicating the lowest level and 20 the highest level of rhythmicity. Significance levels were adjusted for multiple comparisons (total of 40 comparisons, for signal strength and spatial extent; * significant at adjusted alpha level: $p < .00125$).

The results of the RI-ranking were replicated to a large extent by complementary analyses using thresholds of $z \geq 1.0$ and $z \geq 2.0$, and the mask based approach: in either analysis ICs 5, 11, and 13 were among the four highest ranked connectivity patterns, whereas IC 6 and 18 ranged across the four most stable ones (except of IC 18 in case of the mask based approach; see Appendix C for further information).

Discussion

Here, we investigated whether fMRI derived connectivity patterns – controlled for internal time and for time awake – vary systematically over the course of a day under resting-state conditions. Our results demonstrate that the degree of daily modulation (quantified as Rhythmicity Index, RI, see Experimental procedures) varies largely across resting-state connectivity patterns, ranging from highly rhythmic to stable.

According to the cut-off criterion (RI > mean RI + 1.5 SD), highly rhythmic connectivity patterns regarding their connectivity strength included two sub-systems of the Default-Mode Network (DMN: ICs 5 & 17) and a network extending over sensorimotor regions (IC 11). Both sub-systems of the DMN were also significantly rhythmic in their spatial extent. One of the most stable connectivity patterns (IC 18) was considered to represent non-neural physiological noise derived from large vessel pulsations and the other most stable pattern (IC 6) represented a RSN mainly extending over frontal cortical areas. The ranking of connectivity patterns by RI was to a large extent consistent across complementary analyses.

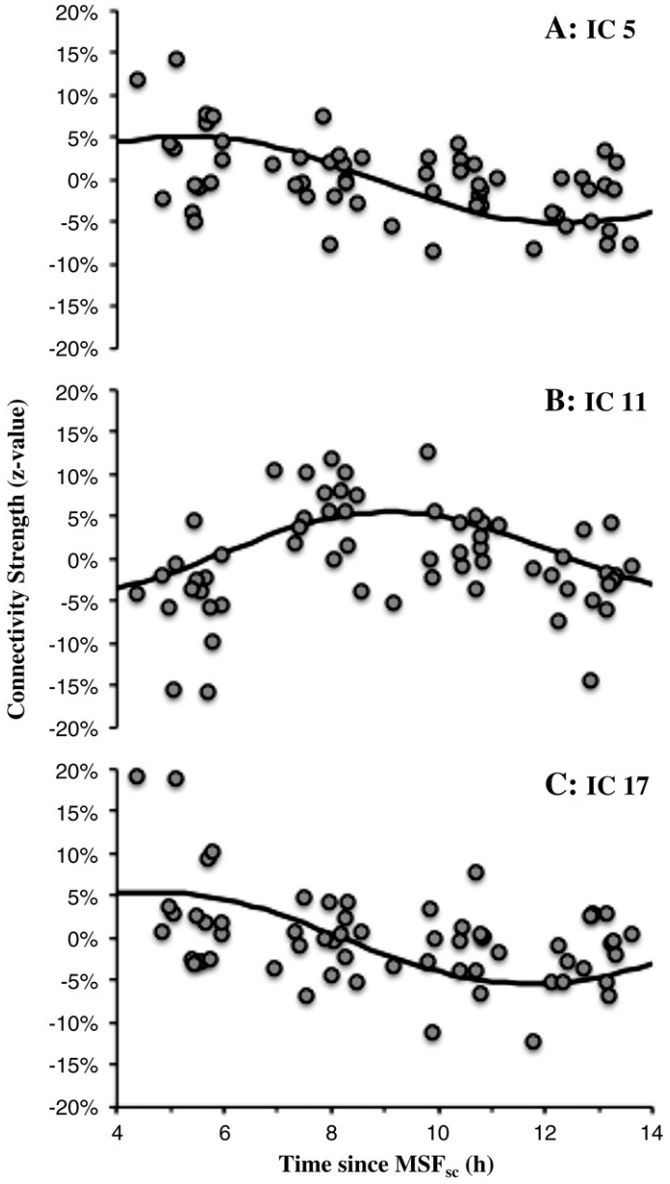

Fig. 4. Time course of connectivity strength within rhythmic connectivity patterns. The figure demonstrates % deviations of mean z-values characterizing the connectivity strength within individual connectivity patterns thresholded at $z \geq 3.0$ achieved at sessions 1–4 from the individual mean z-value (of that connectivity pattern) across all 4 sessions (gray dots), and the significant fit ($p < 0.001$, corrected for multiple comparisons) of the applied two-harmonic regression model (solid line). Data are shown for the rhythmic connectivity patterns represented in IC 5 (A), 11 (B), and 17 (C). % deviations from the individual mean z-value are plotted against time (in h) elapsed since MSF$_{sc}$.

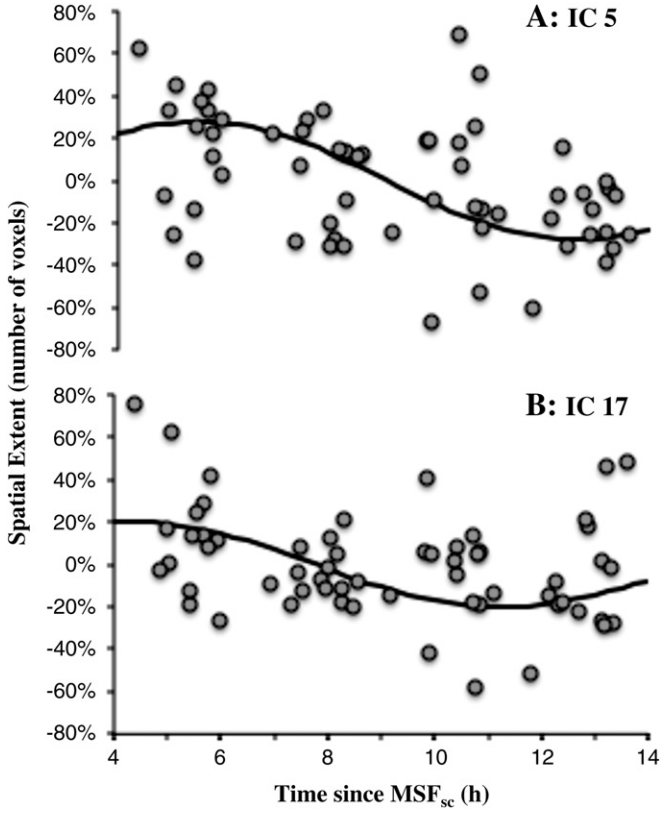

Fig. 5. Time course of spatial extent within rhythmic connectivity patterns. The figure demonstrates % deviations of the number of voxels characterizing the spatial extent of an individual connectivity pattern thresholded at $z \geq 3.0$ achieved at sessions 1–4 from the individual mean number of voxels (of that connectivity pattern) across all 4 sessions (gray dots), and the fit of the applied two-harmonic regression model (solid line). Data are shown for the rhythmic connectivity patterns represented in IC 5 (A) and 17 (B). % deviations from the individual mean number of voxels are plotted against time (in h) elapsed since MSF$_{sc}$.

The two-harmonic fits to the daily time courses in connectivity strength were significant not only for ICs 5, 11, and 17, but also for IC 13 (the fourth in the ranking), the RI of which fell however below the cut-off and was therefore not classified as 'highly rhythmic'. In contrast, the spatial extent of the connectivity patterns produced no significant fits after Bonferroni correction for multiple regressions (possibly because the recruited number of voxels showed a much higher variation than in the case of connectivity strength; see Appendix A for further information).

The DMN is usually most active during passive settings and has therefore been proposed to participate in a wide range of internally directed processes (Buckner et al., 2008; Gusnard et al., 2001; Mason et al., 2007). Four connectivity patterns (IC 5, 14, 16 & 17) found in this study have been described as sub-networks of the DMN (Zuo et al., 2010); this is little surprise since recent reports have indicated that different components of the DMN are differentially specialized thereby forming DMN sub-systems (Buckner et al., 2008; Laird et al., 2009; Spreng et al., 2009). All four sub-networks of the DMN overlapped in the posterior cingulate cortex, a structure known for its extensive connectivity with other DMN nodes. It can therefore be considered as a "functional hub" within this network (Laird et al., 2009).

The time courses of functional connectivity of the rhythmic DMN sub-systems (ICs 5 & 17) oscillated in phase for both connectivity strength and spatial extent, in each case peaking early in the morning (in reference to individual internal time) and declining thereafter. In addition to their similar time courses, both networks strongly overlapped in the spatial extent (mainly including the precuneus, the posterior cingulate cortex, the medial temporal gyrus, and the inferior parietal lobule). Sub-systems of this network – with the majority of nodes located in the posterior cerebral regions as in this case – have been associated with *somesthesis*, describing the processing of sensory inputs from various tissues (Laird et al., 2009). Given that the vast majority of biological functions show daily fluctuations, it is conceivable that the central processing of rhythmic interoceptive inputs may also be rhythmic. The observations that pain perception – linked to activation of the DMN (Ter Minassian et al., 2012) – varies across the day (Folkard et al., 1976; Strian et al., 1989) support this hypothesis.

The RSN represented in IC 11 has consistently been described in various resting-state fMRI studies (Beckmann et al., 2005; Biswal et al., 2010; Damoiseaux et al., 2006; Laird et al., 2011; Smith et al., 2009) and is known to correspond to brain areas strongly involved in a wide range of motor and somatosensory processes (Laird et al., 2011; Smith et al., 2009). A daily modulation in brain structures associated with

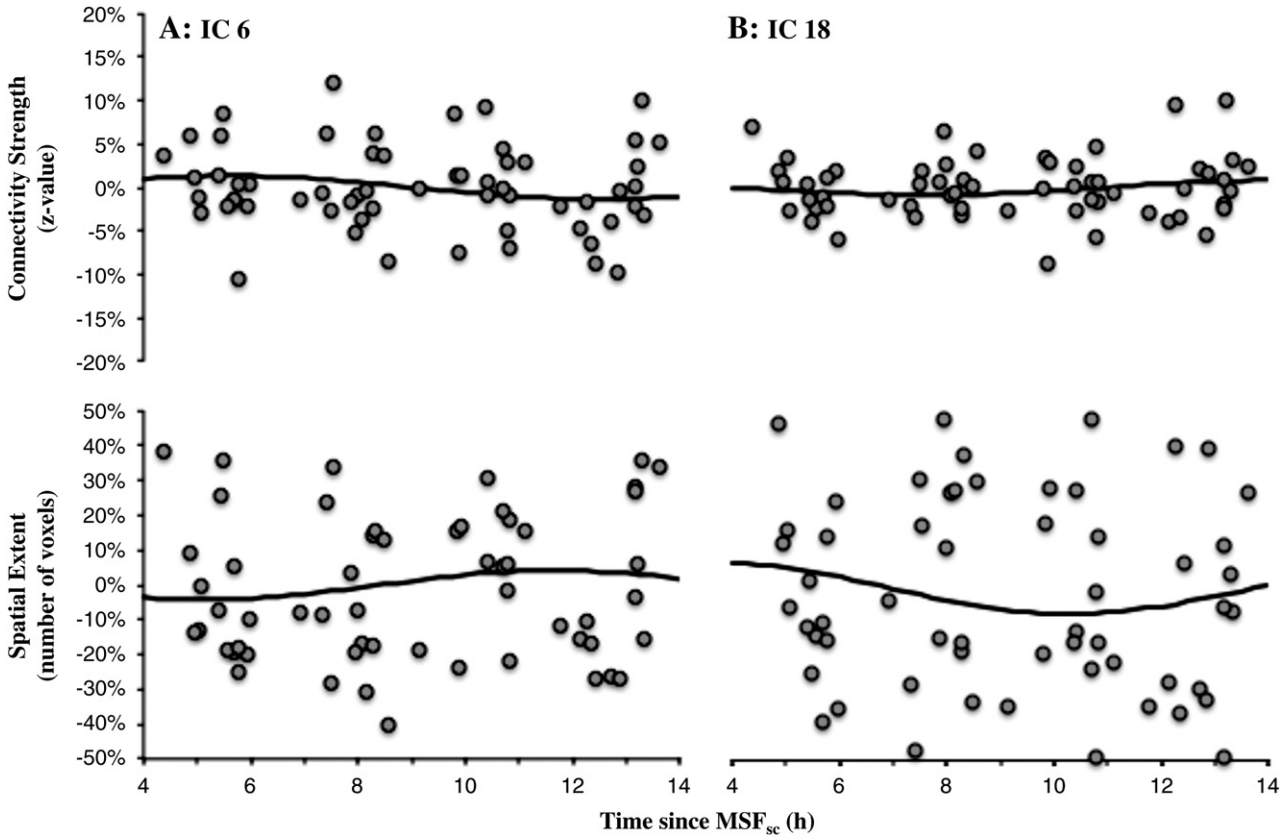

Fig. 6. Time course of connectivity strength and spatial extent within stable connectivity patterns. Equivalent to Figs. 4 and 5, Fig. 6 depicts the time course of connectivity strength (upper row) and the spatial extent (lower row) in the most stable connectivity patterns represented in IC 6 (A, left column) and IC 18 (B, right column).

motor and somatosensory functions – though not confirmed by the outlier criterion in the spatial extent analysis – is supported by our previous report of time-of-day influences on these regions during a finger-tapping task (Peres et al., 2011) as well as by the fact that motor and somatosensory functions per se are subject to daily rhythmicity, e.g., for handwriting (Jasper et al., 2009a,b; Moussay et al., 2002), finger-tapping and cycling (Moussay et al., 2002) or proprioception (Miller et al., 1992). Daily rhythmicity in brain structures usually involved in motor and somatosensory processing could also explain the high rhythmicity rank of the RSN mainly involving the basal ganglia, the thalami, and the cerebellum (IC 13, fourth highest ranked with regard to connectivity strength and spatial extent, respectively), despite its RI below the cut-off. As with the brain regions localized in IC 11, the subcortical structures of this network have been associated with a wide range of motor and somatosensory processes (Laird et al., 2011; Smith et al., 2009).

The connectivity pattern represented in IC 6 has been repeatedly reported to correspond to cortical regions that play a major role in executive control (Beckmann et al., 2005; Damoiseaux et al., 2006; Laird et al., 2011; Miller and Cohen, 2001). This cognitive domain comprises a variety of cognitive processes known to be influenced by time-of-day (Schmidt et al., 2007). However, under special circumstances, such as non-challenging tasks, executive control may remain constant across the day (Schmidt et al., 2007). Since our participants were – in line with other resting-state fMRI studies – instructed not to think of anything in particular, this could certainly be classified as a non-challenging task. Accordingly, the time course of functional connectivity should remain stable in a RSN associated with executive control.

Fluctuations in the low-frequency domain of the BOLD signal – where resting-state fluctuations are detected – are known to be significantly influenced by low-frequency fluctuations in end-tidal Carbon dioxide (Wise et al., 2004) and natural variations in the depth and rate of respiration (Birn et al., 2006, 2008), which both are highly correlated and partially explain the BOLD signal variance across the brain (Chang and Glover, 2009). Variations in breathing rate and depth impact the BOLD signal especially in regions with high blood volume as the cerebral gray matter including areas forming the DMN (Birn et al., 2006) and may not be completely removable by ICA (Birn et al., 2008). A similar effect on the BOLD signal variance was also found for low-frequency fluctuations in the cardiac rate, especially in brain areas referring to the DMN (Shmueli et al., 2007). Therefore, it has been proposed to monitor the cardiac and respiratory functions in order to model and remove the confounding physiological noise resulting in less BOLD signal variance and therefore significantly altered DMN connectivity maps (Birn et al., 2008; Chang et al., 2009; Glover et al., 2000).

Low-frequency fluctuations in respiratory and cardiac function may have influenced the 16 RSNs presented in this work since cardiovascular and respiratory parameters were not monitored. It is therefore possible that the observed daily modulation of functional connectivity in specific RSNs, especially in both sub-systems of the DMN, may be affected by circadian rhythms in physiological parameters, especially since the presence of robust circadian rhythms in heart function such as heart rate or heart rate variability (Furlan et al., 1990; Huikuri et al., 1994; Malpas and Purdie, 1990; Vandewalle et al., 2007b) as well as in respiratory function, for example resting pulmonary ventilation or breathing rate (see for review Mortola, 2004) has been repeatedly demonstrated.

We believe however that our demonstration of daily modulations in only few RSNs is based on specific rhythmicity in neural processing rather than on general influences of rhythmic physiological 'noise'. If that was the case, all connectivity patterns should be affected, which our results disprove. In addition, general physiology should produce daily modulations especially in connectivity patterns associated with physiological noise (ICs 1, 2, 9, and 18) rather than in those

repeatedly described as RSNs. Notably, the "noise" patterns in our study predominantly ranked as stable.

Although the reasons for the different degrees of daily modulation across resting-state connectivity patterns remain speculative, our results should be considered when interpreting resting-state fMRI data (and most probably also other fMRI results). This holds especially for clinical questions; analyses of the DMN – often presumed to represent associated pathologic conditions in the intrinsic brain function of clinical populations – may be misinterpreted when its inherent rhythmicity, individual chronotype, time awake and/or the local time of examination are not taken into account.

Conclusion

The degree of daily modulation largely varies across fMRI derived resting-state connectivity patterns, ranging from highly rhythmic to stable. Our results suggest that these daily modulations are based on neural rhythmicity rather than on a general rhythmicity in physiological 'noise'. The most rhythmic RSNs are associated with motor and somatosensory processes as well as with the processing of various sensory inputs from various tissues. In contrast, the RSN mainly associated with executive control is the most stable connectivity pattern. Although the reasons for the presented findings remain speculative, their impact should be considered in the interpretation of both scientific and clinical fMRI studies.

Acknowledgments

A grant from the university's own FoeFoLe program funded this research (Grant number 651). I. P. was supported by a research scholarship of the Elite Network of Bavaria. The authors thank Petra Carl for excellent organizational assistance and Dirk Spannhake for his competent work.

Conflict of interest

The authors declare no conflict of interest.

Appendix A. Supplementary data

Supplementary data to this article can be found online at http://dx.doi.org/10.1016/j.neuroimage.2012.08.010.

References

Andersson, J.L., Hutton, C., Ashburner, J., Turner, R., Friston, K., 2001. Modeling geometric deformations in EPI time series. Neuroimage 13, 903–919.
Beckmann, C.F., DeLuca, M., Devlin, J.T., Smith, S.M., 2005. Investigations into resting-state connectivity using independent component analysis. Philos. Trans. R. Soc. Lond. B Biol. Sci. 360, 1001–1013.
Beckmann, C.F., Mackay, C.E., Filippini, N., Smith, S.M., 2009. Group comparison of resting-state FMRI data using multi-subject ICA and dual regression. OHBM poster.
Birn, R.M., Diamond, J.B., Smith, M.A., Bandettini, P.A., 2006. Separating respiratory-variation-related fluctuations from neuronal-activity-related fluctuations in fMRI. Neuroimage 31, 1536–1548.
Birn, R.M., Smith, M.A., Jones, T.B., Bandettini, P.A., 2008. The respiration response function: the temporal dynamics of fMRI signal fluctuations related to changes in respiration. Neuroimage 40, 644–654.
Biswal, B., Yetkin, F.Z., Haughton, V.M., Hyde, J.S., 1995. Functional connectivity in the motor cortex of resting human brain using echo-planar MRI. Magn. Reson. Med. 34, 537–541.
Biswal, B.B., Mennes, M., Zuo, X.N., Gohel, S., Kelly, C., Smith, S.M., Beckmann, C.F., Adelstein, J.S., Buckner, R.L., Colcombe, S., Dogonowski, A.M., Ernst, M., Fair, D., Hampson, M., Hoptman, M.J., Hyde, J.S., Kiviniemi, V.J., Kotter, R., Li, S.J., Lin, C.P., Lowe, M.J., Mackay, C., Madden, D.J., Madsen, K.H., Margulies, D.S., Mayberg, H.S., McMahon, K., Monk, C.S., Mostofsky, S.H., Nagel, B.J., Pekar, J.J., Peltier, S.J., Petersen, S.E., Riedl, V., Rombouts, S.A., Rypma, B., Schlaggar, B.L., Schmidt, S., Seidler, R.D., Siegle, G.J., Sorg, C., Teng, G.J., Veijola, J., Villringer, A., Walter, M., Wang, L., Weng, X.C., Whitfield-Gabrieli, S., Williamson, P., Windischberger, C., Zang, Y.F., Zhang, H.Y., Castellanos, F.X., Milham, M.P., 2010. Toward discovery science of human brain function. Proc. Natl. Acad. Sci. U. S. A. 107, 4734–4739.
Boly, M., Phillips, C., Balteau, E., Schnakers, C., Degueldre, C., Moonen, G., Luxen, A., Peigneux, P., Faymonville, M.E., Maquet, P., Laureys, S., 2008. Consciousness and cerebral baseline activity fluctuations. Hum. Brain Mapp. 29, 868–874.
Borbely, A.A., 1982. A two process model of sleep regulation. Hum. Neurobiol. 1, 195–204.
Box, E.P., Jenkins, G.M., 1970. Time series analysis. Forecasting and Control.Holden-Day, San Francisco (553 pp.).
Brookes, M.J., Woolrich, M., Luckhoo, H., Price, D., Hale, J.R., Stephenson, M.C., Barnes, G.R., Smith, S.M., Morris, P.G., 2011. Investigating the electrophysiological basis of resting state networks using magnetoencephalography. Proc. Natl. Acad. Sci. U. S. A. 108, 16783–16788.
Brown, E.N., Czeisler, C.A., 1992. The statistical analysis of circadian phase and amplitude in constant-routine core-temperature data. J. Biol. Rhythms 7, 177–202.
Buckner, R.L., Andrews-Hanna, J.R., Schacter, D.L., 2008. The brain's default network: anatomy, function, and relevance to disease. Ann. N. Y. Acad. Sci. 1124, 1–38.
Buysse, D.J., Nofzinger, E.A., Germain, A., Meltzer, C.C., Wood, A., Ombao, H., Kupfer, D.J., Moore, R.Y., 2004. Regional brain glucose metabolism during morning and evening wakefulness in humans: preliminary findings. Sleep 27, 1245–1254.
Cagnacci, A., Elliott, J.A., Yen, S.S., 1992. Melatonin: a major regulator of the circadian rhythm of core temperature in humans. J. Clin. Endocrinol. Metab. 75, 447–452.
Chang, C., Glover, G.H., 2009. Relationship between respiration, end-tidal CO_2, and BOLD signals in resting-state fMRI. Neuroimage 47, 1381–1393.
Chang, C., Cunningham, J.P., Glover, G.H., 2009. Influence of heart rate on the BOLD signal: the cardiac response function. Neuroimage 44, 857–869.
Czeisler, C.A., Klerman, E.B., 1999. Circadian and sleep-dependent regulation of hormone release in humans. Recent Prog. Horm. Res. 54, 97–130 (discussion 130–132).
Dagli, M.S., Ingeholm, J.E., Haxby, J.V., 1999. Localization of cardiac-induced signal change in fMRI. Neuroimage 9, 407–415.
Damoiseaux, J.S., Rombouts, S.A., Barkhof, F., Scheltens, P., Stam, C.J., Smith, S.M., Beckmann, C.F., 2006. Consistent resting-state networks across healthy subjects. Proc. Natl. Acad. Sci. U. S. A. 103, 13848–13853.
Drobnjak, I., Gavaghan, D., Suli, E., Pitt-Francis, J., Jenkinson, M., 2006. Development of a functional magnetic resonance imaging simulator for modeling realistic rigid-body motion artifacts. Magn. Reson. Med. 56, 364–380.
Filippini, N., MacIntosh, B.J., Hough, M.G., Goodwin, G.M., Frisoni, G.B., Smith, S.M., Matthews, P.M., Beckmann, C.F., Mackay, C.E., 2009. Distinct patterns of brain activity in young carriers of the APOE-epsilon4 allele. Proc. Natl. Acad. Sci. U. S. A. 106, 7209–7214.
Folkard, S., Glynn, C.J., Lloyd, J.W., 1976. Diurnal variation and individual differences in the perception of intractable pain. J. Psychosom. Res. 20, 289–301.
Fox, M.D., Snyder, A.Z., Vincent, J.L., Corbetta, M., Van Essen, D.C., Raichle, M.E., 2005. The human brain is intrinsically organized into dynamic, anticorrelated functional networks. Proc. Natl. Acad. Sci. U. S. A. 102, 9673–9678.
Fox, M.D., Corbetta, M., Snyder, A.Z., Vincent, J.L., Raichle, M.E., 2006. Spontaneous neuronal activity distinguishes human dorsal and ventral attention systems. Proc. Natl. Acad. Sci. U. S. A. 103, 10046–10051.
Furlan, R., Guzzetti, S., Crivellaro, W., Dassi, S., Tinelli, M., Baselli, G., Cerutti, S., Lombardi, F., Pagani, M., Malliani, A., 1990. Continuous 24-hour assessment of the neural regulation of systemic arterial pressure and RR variabilities in ambulant subjects. Circulation 81, 537–547.
Glover, G.H., Li, T.Q., Ress, D., 2000. Image-based method for retrospective correction of physiological motion effects in fMRI: RETROICOR. Magn. Reson. Med. 44, 162–167.
Greicius, M.D., Krasnow, B., Reiss, A.L., Menon, V., 2003. Functional connectivity in the resting brain: a network analysis of the default mode hypothesis. Proc. Natl. Acad. Sci. U. S. A. 100, 253–258.
Greicius, M.D., Srivastava, G., Reiss, A.L., Menon, V., 2004. Default-mode network activity distinguishes Alzheimer's disease from healthy aging: evidence from functional MRI. Proc. Natl. Acad. Sci. U. S. A. 101, 4637–4642.
Gusnard, D.A., Akbudak, E., Shulman, G.L., Raichle, M.E., 2001. Medial prefrontal cortex and self-referential mental activity: relation to a default mode of brain function. Proc. Natl. Acad. Sci. U. S. A. 98, 4259–4264.
He, B.J., Snyder, A.Z., Zempel, J.M., Smyth, M.D., Raichle, M.E., 2008. Electrophysiological correlates of the brain's intrinsic large-scale functional architecture. Proc. Natl. Acad. Sci. U. S. A. 105, 16039–16044.
Horovitz, S.G., Braun, A.R., Carr, W.S., Picchioni, D., Balkin, T.J., Fukunaga, M., Duyn, J.H., 2009. Decoupling of the brain's default mode network during deep sleep. Proc. Natl. Acad. Sci. U. S. A. 106, 11376–11381.
Huikuri, H.V., Niemela, M.J., Ojala, S., Rantala, A., Ikaheimo, M.J., Airaksinen, K.E., 1994. Circadian rhythms of frequency domain measures of heart rate variability in healthy subjects and patients with coronary artery disease. Effects of arousal and upright posture. Circulation 90, 121–126.
Jasper, I., Haussler, A., Baur, B., Marquardt, C., Hermsdorfer, J., 2009a. Circadian variations in the kinematics of handwriting and grip strength. Chronobiol. Int. 26, 576–594.
Jasper, I., Haussler, A., Marquardt, C., Hermsdorfer, J., 2009b. Circadian rhythm in handwriting. J. Sleep Res. 18, 264–271.
Jenkinson, M., Bannister, P., Brady, M., Smith, S., 2002. Improved optimization for the robust and accurate linear registration and motion correction of brain images. Neuroimage 17, 825–841.
Kenagy, G.J., 1980. CenterKenagy, G.J., 1980. CenterKenagy, G.J., 1980. CenterKenagy, G.J., 1980. CenterKenagy, G.J., 1980. CenterKenagy, G.J., 1980. Center.
Laird, A.R., Eickhoff, S.B., Li, K., Robin, D.A., Glahn, D.C., Fox, P.T., 2009. Investigating the functional heterogeneity of the default mode network using coordinate-based meta-analytic modeling. J. Neurosci. 29, 14496–14505.
Laird, A.R., Fox, P.M., Eickhoff, S.B., Turner, J.A., Ray, K.L., McKay, D.R., Glahn, D.C., Beckmann, C.F., Smith, S.M., Fox, P.T., 2011. Behavioral interpretations of intrinsic connectivity networks. J. Cogn. Neurosci.

Lund, T.E., Madsen, K.H., Sidaros, K., Luo, W.L., Nichols, T.E., 2006. Non-white noise in fMRI: does modelling have an impact? Neuroimage 29, 54–66.
Malpas, S.C., Purdie, G.L., 1990. Circadian variation of heart rate variability. Cardiovasc. Res. 24, 210–213.
Mason, M.F., Norton, M.I., Van Horn, J.D., Wegner, D.M., Grafton, S.T., Macrae, C.N., 2007. Wandering minds: the default network and stimulus-independent thought. Science 315, 393–395.
Merrow, M., Spoelstra, K., Roenneberg, T., 2005. The circadian cycle: daily rhythms from behaviour to genes. EMBO Rep. 6, 930–935.
Miall, R.C., Robertson, E.M., 2006. Functional imaging: is the resting brain resting? Curr. Biol. 16, R998–1000.
Miller, E.K., Cohen, J.D., 2001. An integrative theory of prefrontal cortex function. Annu. Rev. Neurosci. 24, 167–202.
Miller, L.S., Lombardo, T.W., Fowler, S.C., 1992. Time of day effects on a human force discrimination task. Physiol. Behav. 52, 839–841.
Mortola, J.P., 2004. Breathing around the clock: an overview of the circadian pattern of respiration. Eur. J. Appl. Physiol. 91, 119–129.
Moussay, S., Dosseville, F., Gauthier, A., Larue, J., Sesboue, B., Davenne, D., 2002. Circadian rhythms during cycling exercise and finger-tapping task. Chronobiol. Int. 19, 1137–1149.
Oldfield, R.C., 1971. The assessment and analysis of handedness: the Edinburgh inventory. Neuropsychologia 9, 97–113.
Peres, I., Vetter, C., Blautzik, J., Reiser, M., Pöppel, E., Meindl, T., Roenneberg, T., Gutyrchik, E., 2011. Chronotype predicts activity patterns in the neural underpinnings of the motor system during the day. Chronobiol. Int. 28, 883–889.
Pizoli, C.E., Shah, M.N., Snyder, A.Z., Shimony, J.S., Limbrick, D.D., Raichle, M.E., Schlaggar, B.L., Smyth, M.D., 2011. Resting-state activity in development and maintenance of normal brain function. Proc. Natl. Acad. Sci. U. S. A. 108, 11638–11643.
Raichle, M.E., MacLeod, A.M., Snyder, A.Z., Powers, W.J., Gusnard, D.A., Shulman, G.L., 2001. A default mode of brain function. Proc. Natl. Acad. Sci. U. S. A. 98, 676–682.
Refinetti, R., Menaker, M., 1992. The circadian rhythm of body temperature. Physiol. Behav. 51, 613–637.
Rocca, M.A., Valsasina, P., Absinta, M., Riccitelli, G., Rodegher, M.E., Misci, P., Rossi, P., Falini, A., Comi, G., Filippi, M., 2010. Default-mode network dysfunction and cognitive impairment in progressive MS. Neurology 74, 1252–1259.
Roenneberg, T., Foster, R.G., 1997. Twilight times: light and the circadian system. Photochem. Photobiol. 66, 549–561.
Roenneberg, T., Merrow, M., 2005. Circadian clocks—the fall and rise of physiology. Nat. Rev. Mol. Cell Biol. 6, 965–971.
Roenneberg, T., Taylor, W., 2000. Automated recordings of bioluminescence with special reference to the analysis of circadian rhythms. Methods Enzymol. 305, 104–119.
Roenneberg, T., Wirz-Justice, A., Merrow, M., 2003. Life between clocks: daily temporal patterns of human chronotypes. J. Biol. Rhythms 18, 80–90.
Roenneberg, T., Kuehnle, T., Juda, M., Kantermann, T., Allebrandt, K., Gordijn, M., Merrow, M., 2007. Epidemiology of the human circadian clock. Sleep Med. Rev. 11, 429–438.
Roenneberg, T., Allebrandt, K.V., Merrow, M., Vetter, C., 2012. Social jetlag and obesity. Curr. Biol. 22, 939–943.
Rogers, N.L., Dorrian, J., Dinges, D.F., 2003. Sleep, waking and neurobehavioural performance. Front. Biosci. 8, s1056–1067.
Rombouts, S.A., Barkhof, F., Goekoop, R., Stam, C.J., Scheltens, P., 2005. Altered resting state networks in mild cognitive impairment and mild Alzheimer's disease: an fMRI study. Hum. Brain Mapp. 26, 231–239.
Schmidt, C., Collette, F., Cajochen, C., Peigneux, P., 2007. A time to think: circadian rhythms in human cognition. Cogn. Neuropsychol. 24, 755–789.
Schmidt, C., Collette, F., Leclercq, Y., Sterpenich, V., Vandewalle, G., Berthomier, P., Berthomier, C., Phillips, C., Tinguely, G., Darsaud, A., Gais, S., Schabus, M., Desseilles, M., Dang-Vu, T.T., Salmon, E., Balteau, E., Degueldre, C., Luxen, A., Maquet, P., Cajochen, C., Peigneux, P., 2009. Homeostatic sleep pressure and responses to sustained attention in the suprachiasmatic area. Science 324, 516–519.
Shmuel, A., Leopold, D.A., 2008. Neuronal correlates of spontaneous fluctuations in fMRI signals in monkey visual cortex: Implications for functional connectivity at rest. Hum. Brain Mapp. 29, 751–761.
Smith, S.M., 2002. Fast robust automated brain extraction. Hum. Brain Mapp. 17, 143–155.
Smith, S.M., Fox, P.T., Miller, K.L., Glahn, D.C., Fox, P.M., Mackay, C.E., Filippini, N., Watkins, K.E., Toro, R., Laird, A.R., Beckmann, C.F., 2009. Correspondence of the brain's functional architecture during activation and rest. Proc. Natl. Acad. Sci. U. S. A. 106, 13040–13045.
Sorg, C., Riedl, V., Muhlau, M., Calhoun, V.D., Eichele, T., Laer, L., Drzezga, A., Forstl, H., Kurz, A., Zimmer, C., Wohlschlager, A.M., 2007. Selective changes of resting-state networks in individuals at risk for Alzheimer's disease. Proc. Natl. Acad. Sci. U. S. A. 104, 18760–18765.
Spreng, R.N., Mar, R.A., Kim, A.S., 2009. The common neural basis of autobiographical memory, prospection, navigation, theory of mind, and the default mode: a quantitative meta-analysis. J. Cogn. Neurosci. 21, 489–510.
Stigler, K.A., McDonald, B.C., Anand, A., Saykin, A.J., McDougle, C.J., 2011. Structural and functional magnetic resonance imaging of autism spectrum disorders. Brain Res. 1380, 146–161.
Strian, F., Lautenbacher, S., Galfe, G., Holzl, R., 1989. Diurnal variations in pain perception and thermal sensitivity. Pain 36, 125–131.
Ter Minassian, A., Ricalens, E., Humbert, S., Duc, F., Aube, C., Beydon, L., 2012. Dissociating anticipation from perception: acute pain activates default mode network. Hum. Brain Mapp.
Toth, M., Kiss, A., Kosztolanyi, P., Kondakor, I., 2007. Diurnal alterations of brain electrical activity in healthy adults: a LORETA study. Brain Topogr. 20, 63–76.
Vandewalle, G., Balteau, E., Phillips, C., Degueldre, C., Moreau, V., Sterpenich, V., Albouy, G., Darsaud, A., Desseilles, M., Dang-Vu, T.T., Peigneux, P., Luxen, A., Dijk, D.J., Maquet, P., 2006. Daytime light exposure dynamically enhances brain responses. Curr. Biol. 16, 1616–1621.
Vandewalle, G., Gais, S., Schabus, M., Balteau, E., Carrier, J., Darsaud, A., Sterpenich, V., Albouy, G., Dijk, D.J., Maquet, P., 2007a. Wavelength-dependent modulation of brain responses to a working memory task by daytime light exposure. Cereb. Cortex 17, 2788–2795.
Vandewalle, G., Middleton, B., Rajaratnam, S.M., Stone, B.M., Thorleifsdottir, B., Arendt, J., Dijk, D.J., 2007b. Robust circadian rhythm in heart rate and its variability: influence of exogenous melatonin and photoperiod. J. Sleep Res. 16, 148–155.
Vincent, J.L., Patel, G.H., Fox, M.D., Snyder, A.Z., Baker, J.T., Van Essen, D.C., Zempel, J.M., Snyder, L.H., Corbetta, M., Raichle, M.E., 2007. Intrinsic functional architecture in the anaesthetized monkey brain. Nature 447, 83–86.
Wise, R.G., Ide, K., Poulin, M.J., Tracey, I., 2004. Resting fluctuations in arterial carbon dioxide induce significant low frequency variations in BOLD signal. Neuroimage 21, 1652–1664.
Wittmann, M., Dinich, J., Merrow, M., Roenneberg, T., 2006. Social jetlag: misalignment of biological and social time. Chronobiol. Int. 23, 497–509.
Zhang, H.Y., Wang, S.J., Liu, B., Ma, Z.L., Yang, M., Zhang, Z.J., Teng, G.J., 2010. Resting brain connectivity: changes during the progress of Alzheimer disease. Radiology 256, 598–606.
Zuo, X.N., Kelly, C., Adelstein, J.S., Klein, D.F., Castellanos, F.X., Milham, M.P., 2010. Reliable intrinsic connectivity networks: test–retest evaluation using ICA and dual regression approach. Neuroimage 49, 2163–2177.